One dimensional steady-state modeling of spray detonations considering loss effects

Nicolas Tricard* and Xinyu Zhao†
University of Connecticut, Storrs, CT, 06269

Steady-state one-dimensional droplet-laden detonations are modeled in this study. Two-way coupling of droplet and gaseous species is considered, and combustion is modeled using detailed chemistry supplied through the Cantera chemistry interface as done by Lu and Law [1]. The steady state detonation velocities are computed through a guess and check approach. Heat and friction losses to the walls are included, and their effects on the detonation velocity are studied through parametric variations of loss coefficients. Quenching characteristics are defined as the turning point in steady state velocities in the loss curves. The sensitivities of detonation velocity to the droplet diameters are also investigated, indicating a non-monotonic behavior. Increasing droplet diameters results in detonation quenching at higher loss coefficients. Between the two fuels, heptane shows a greater resilience to external heat and friction losses than JP10. The faster vaporization and thermal runaway of heptane results in an earlier CJ state and decreased integrated external losses. JP10, however, shows earlier onset of vaporization-limited detonations, due to its relatively low volatility.

I. Nomenclature

L	=	Length (m)
q	=	Heat Flux (W/m^2)
ρ	=	Density (kg/m^3)
u	=	Velocity (m/s)
p	=	Pressure (Pa)
$\dot{m}''$	=	Mass Flux (kg/m$^2 s$)
h	=	Enthalpy (J/kg)
h_0	=	Enthalpy of Formation at Standard State (J/kg)
x	=	Distance (m)
f	=	Drag (kg/m^{2}s^2)
$\dot{m}_v$	=	Droplet Vaporization Rate (kg/m$^3 s$)
ω_k	=	Production Rate of Species k
D	=	Detonation Velocity (m/s)
Y_k	=	Mass Fraction of Species k
X_k	=	Mole Fraction of Species k
r_d	=	Droplet Radius (m)
W	=	Molecular Weight (kg/mol)
C_d	=	Drag Coefficient (m)
C_h	=	Heat Loss Coefficient (m)
Re	=	Reynolds Number
Pr	=	Prandtl Number
c_p	=	Specific Heat at Constant Pressure (J/kgK)
c_v	=	Specific Heat at Constant Volume(J/kgK)
$l^\star$	=	Characteristic Length
λ_g	=	Gas Thermal Conductivity (W/mK)
n_d	=	Droplet Number Density (droplets/m^3)

*Graduate Research Assistant, University of Connecticut, Mechanical Engineering, 191 Auditorium Rd Unit 3139, Storrs, CT 06269, AIAA student member.

†Associate Professor, University of Connecticut, Mechanical Engineering, 191 Auditorium Rd Unit 3139, Storrs, CT 06269, AIAA member.

L = Length (m)
Le = Lewis Number (m)
B_Y = Spalding Mass Transfer Number
B_Y = Spalding Heat Transfer Number
R_g = Gas Constant (J/kgK)
γ = Ratio of Specific Heats
K = Number of Species

II. Introduction

Detonation has been receiving considerable attention in recent years. Detonations involve the ignition of a fuel/oxidizer mixture as a result of a passing shock wave. Traditional one dimensional detonation models contain an initial normal shock, followed by a virtually instantaneous increase in pressure, density and temperature. These post-shock conditions cause the mixture to subsequently react, increasing the Mach number until it reaches a value of unity. This marks the end of the so-called Zel'dovich, von Neumann and Döring detonation (ZND detonation) [2]. The one-dimensional conservation equations in differential form can be used to model this process numerically.

Liquid-fueled detonations are generally considered to be more applicable than gaseous detonations because most jet fuels are provided in the liquid form. Modeling of liquid fueled detonations is a complex problem that demands simultaneous modeling of compressible multi-phase transport, phase change, chemical reactions and heat transfer. Spray detonations can be subject to internal loss effects due to the vaporization process and external loss effects due to heat and momentum transfer. In addition, the fuel/oxidizer mixture in the post-shock reaction zone is often inhomogeneous due to simultaneous vaporization and mixing. Therefore, spray detonation modeling requires robust chemical kinetic models that are valid over a wide range of thermochemical states. Whereas in the past this was not possible [3–6], with recent advancement of computational power and chemical kinetic modeling, skeletal or reduced chemical models have been created to address this issue. Kailasanath [7] provided a comprehensive review of spray detonation research in 2006. Recent research has included higher fidelity multi-dimensional simulations of spray detonations with full compressible Navier-Stokes modeling, as well as reduced order but transient models [8–11]. These solvers can be easily adapted to solve one-dimensional spray detonations in a transient manner. However, they can be computationally expensive as marching to steady-state while transporting multiple species is required.

The ZND model has been widely employed to provide a baseline description of the gaseous detonation structure under adiabatic conditions. However, additional formulation can be included to expand the model to include external losses [12]. Lee [2] provides a thorough description on the methods and formulation for including friction and heat loss in a ZND detonation. One key observation made was the existence of a *quenching point* where no further solutions for a steady-state detonation can be found. As the coefficient of wall friction is increased, the steady state detonation velocity decreases. Further increasing the coefficient of wall friction results in a turning point, where no further steady state detonations exist. Instead, the curve wraps around, resulting in multiple solutions of detonation velocity for a given drag coefficient. The existence of a third solution has also been proven mathematically, however, neither the second nor the third solution are stable in nature [2].

To enable general understanding of the internal and external loss effects on structure, quenching and speed in a spray detonation, we extend the ZND model to include mono-dispersed spray detonation in the present study as shown in Fig. 1. The addition of fuel in the liquid phase requires additional formulation to model the condensed phase conservation equations. Additionally, two-way coupling between liquid and gas phases must be accounted for, with source terms for the mass, momentum and energy equations as a result of droplet vaporization, drag, and heating effects. Finally, external friction and heat losses result in additional source terms in the momentum and energy equations and are considered in this study. Lu and Law [1] conducted a study following this method. They studied a heptane-air mixture with varying droplet diameters, loss coefficients, and droplet loadings. Their results outlined the interesting non-monotonic effects from varying these parameters on the detonation structure and quenching characteristics.

The study provided interesting insights and general trends on detonation wave propagation. In this paper, we continue their work by including a new fuel with different volatility: JP10, and we additionally study of the effects of fuel volatility on detonation characteristics. The rest of the paper is organized as follows. A description of the mathematical model and its implementation is provided in Sec. III following those in [1]. Following that, the results are presented and discussed in Sec. IV. Conclusions are finally drawn in Sec. V.

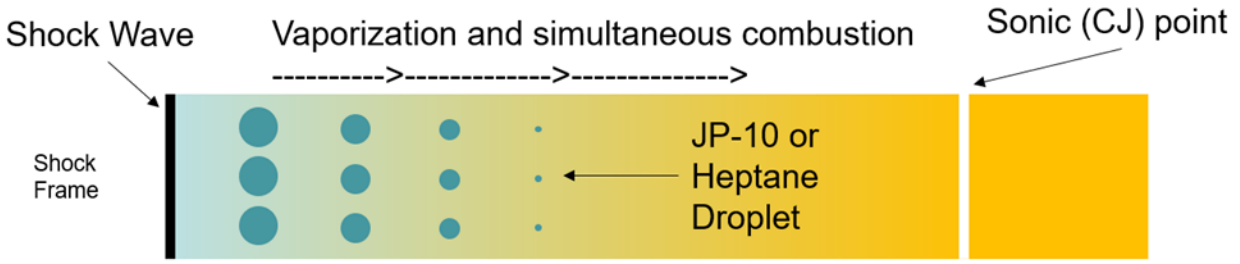

Fig. 1 ZND model with included spray droplets.

III. Mathematical models

The following governing equations are adopted to model the steady-state one-dimensional detonation, following those in Lu and Law [1]. For the gas phase (with subscript "g"), the mass, momentum, energy and species equations read

$$\frac{d(\rho_g u_g)}{dx} = \dot{m}_v, \tag{1}$$

$$\frac{d}{dx}\left(p + \rho_g u_g^2\right) = f_d + f_w + \dot{m}_v u_d, \tag{2}$$

$$\frac{d}{dx}\left[\rho_g u_g \left(h_g + \frac{u_g^2}{2}\right)\right] = f_w D - q_w + f_d u_d - q_d + \dot{m}_v \left(h_{g,f} + \frac{u_d^2}{2}\right), \tag{3}$$

$$\frac{d}{dx}\left(\rho_g u_g Y_{g,k}\right) = \omega_k W_k + \dot{m}_v Y_{d,k} \quad k = 1, ..., K \tag{4}$$

Note the inclusion of the wall friction term in the gas energy equation, Eq. 3 [13]. Additional formulation is adopted to model the spray droplets. The mass, momentum, and energy conservation equations are described as follows.

$$\frac{d}{dx}\left(\rho_d n_d \frac{4}{3}\pi r_d^3 u_d\right) = -\dot{m}_v, \tag{5}$$

$$\frac{d}{dx}\left(\rho_d n_d \frac{4}{3}\pi r_d^3 u_d^2\right) = -f_d - \dot{m}_v u_d, \tag{6}$$

$$\frac{d}{dx}\left[\rho_d n_d \frac{4}{3}\pi r_d^3 u_d^2 \left(h_d + \frac{u_d^2}{2}\right)\right] = q_d - f_d u_d - \dot{m}_v \left(h_{g,f} + \frac{u_d^2}{2}\right). \tag{7}$$

$$\tag{8}$$

The drag and wall losses are modeled by

$$f_d = 4\pi r_d^2 n_d C_{D,d} \rho_g \left|u_g - u_d\right| \left(u_g - u_d\right)/2, \tag{9}$$

$$C_{D,d} = 22 Re_d^{-1}\left(1 + 0.276 Re_d^{\frac{1}{2}} Pr^{\frac{1}{3}}\right), \tag{10}$$

$$f_w = \frac{C_{D,W}}{l^\star}\rho_g \left|D - u_g\right| \left(D - u_g\right)/2, \tag{11}$$

$$q_w = \frac{C_{H,W}}{l^\star}\rho_g \left|D - u_g\right| c_{p,g} \left(T_g - T_w\right). \tag{12}$$

$$\tag{13}$$

Where the wall temperature is equal to the pre-shock temperature of $298K$ in this study. The following equations are used to model the droplet vaporization and heating processes.

$$\dot{m}_v = n_d 4\pi r_d \frac{\lambda_g}{(Le)c_{p,g}} \ln(1+B_Y)\left(1+0.276Re_d^{frac12}Pr^{\frac{1}{3}}\right), \tag{14}$$

$$q_d = n_d 4\pi r_d \frac{\lambda_g}{c_{p,g}} \ln(1+B_H)\left(1+0.276Re_d^{\frac{1}{2}}Pr^{\frac{1}{3}}\right)L, \tag{15}$$

$$Le = \frac{\lambda_g}{\rho_g c_{p,g} D_g}, \tag{16}$$

$$B_Y = \frac{Y_{f,s} - Y_f}{1 - Y_{f,s}}, \tag{17}$$

$$B_H = \frac{c_{p,g}(T_g - T_d)}{L}, \tag{18}$$

$$Y_{f,s} = Y_{f,s}(p, T_d). \tag{19}$$

And finally, the following auxiliary equations are adopted.

$$\frac{d(n_d u_d)}{dx} = 0, \tag{20}$$

$$h_g = \sum_{k=1}^{K} h_{g,k} Y_{g,k}, \tag{21}$$

$$h_{g,k} = (h_{g,k})_0 + \int_{T_0}^{T} c_{p,g,k} dT_g, \tag{22}$$

$$p = \rho_g R_g T_g. \tag{23}$$

From these equations, a system of first order, nonlinear, coupled ODEs can be derived as follows.

$$\frac{du_g}{dx} = \frac{(\gamma-1)M^2 S}{(M^2-1)\rho_g u_g^2}, \tag{24}$$

$$\begin{aligned} S = {} & f_w\left(\frac{\gamma}{\gamma-1}u_g - D\right) + q_w + f_d\left(\frac{\gamma}{\gamma-1}u_g - u_d\right) + q_d \\ & + \sum_{k=1}^{K}\left[\left(h_{g,k} - c_{p,g}T_g\frac{\overline{W}_g}{W_k}\right)\omega_k W_k\right] \\ & + \dot{m}_v\left[\frac{\gamma}{\gamma-1}u_g\left(u_d - u_g\right) - c_{p,g}T_g\frac{\overline{W}_g}{W_f} - \frac{\left(u_d^2 - u_g^2\right)}{2}\right. \\ & \left. + h_{g,f}\left(T_g\right) - h_{g,f}\left(T_d\right)\right], \end{aligned} \tag{25}$$

$$\frac{dT_g}{dx} = -\frac{u_g}{c_{p,g}}\frac{du_g}{dx} + \frac{1}{\rho_g u_g c_{p,g}}[f_w D + f_d u_d - \sum_{k=1}^{K}\left(h_{g,k}\omega_k W_k\right) - q_w - q_d + \dot{m}_v\left[\frac{u_d^2 - u_g^2}{2} - h_{g,f}\left(T_g\right) + h_{g,f}\left(T_d\right)\right]], \tag{26}$$

$$\frac{d\rho_g}{dx} = -\frac{\rho_g}{ug}\frac{du_g}{dx} + \frac{\dot{m}_v}{u_g}, \tag{27}$$

$$\frac{dr_d}{dx} = -\frac{m_v}{\rho_d 4\pi r_d^2 n_d u_d}, \tag{28}$$

$$\frac{du_d}{dx} = -\frac{f_d}{\rho_d \frac{4}{3}\pi r_d^3 n_d u_d}, \tag{29}$$

$$\frac{dT_d}{dx} = \frac{q_d - \dot{m}_v L}{\rho_d \frac{4}{3}\pi r_d^3 n_d u_d c_{v,d}}, \tag{30}$$

$$\frac{dY_{g,k}}{dx} = \frac{1}{\rho_g u_g}\left[\omega_k W_k + \dot{m}_v(Y_{d,k} - Y_{g,k})\right] \quad k = 1, ..., K. \tag{31}$$

The surface mass fraction of fuel used in Eq. 17 is obtained with the knowledge that $X_{f,s} = P_{f,s}/P_g$, where $P_{f,s}$ is calculated from the Antoine equation. Equations. 34 and 35 are the Antoine equations for heptane and JP10, respectively [14]. The Antoine equation parameters for the two vaporization submodels are displayed in Table 1 [15].

$$X_{f,s} = P_{f,s}/P, \tag{32}$$

$$Y_{f,s} = \frac{X_{f,s}W_f}{X_{f,s}W_f - (1 - X_{f,s})\overline{W}_{g,\overline{f}}}. \tag{33}$$

$$\log_{10}(p_{f,s}^{bar}) = A - B/(T_d + C), \tag{34}$$

$$\ln(p_{f,s}^{atm}) = A - B/(T_d + C),, \tag{35}$$

Table 1 Liquid phase model parameters for heptane and JP10.

Parameter	Heptane	JP10
A in Antoine	4.02832	8.173667
B in Antoine	1268.636	2783.0
C in Antoine	-56.199	-117.037
$C_{p,d}$	2236	*
L_v	**	541911.76
ρ_d	680	932

To best represent real fuel properties, empirical formulations for the heptane latent heat of vaporization and the JP10 liquid specific heat are used instead of constant values. The heptane latent heat of vaporization is calculated using Eq. 36. And the JP10 liquid specific heat is calculated empirically using Eq. 37 [16]. The corresponding constants used for Eqs. 36 and 37 are listed in Table 2.

Table 2 Coefficients for the heptane latent heat and the JP10 specific heat empirical equations.

C_1	C_2	C_3	C_4	A	B	T_c
3.3218	0.07975	27.6975	1470	53.66	0.2831	540.2

$$L_{v,hep} = A \exp\left(-B\frac{T_d}{T_c}\right)\left(1 - \frac{T_d}{T_c}\right)^B \tag{36}$$

$$C_{p,d} = R_s\left(C_0 + C_1 T_d^{0.85} + C_2\left(\frac{C_3}{T_d}\right)^2 \frac{\exp\left(C_3 T_d\right)}{\left(\exp\left(C_3/T_d\right) - 1\right)^2}\right) \tag{37}$$

The set of ODEs is implemented and solved with thermodynamic states evaluated through Cantera [17]. For heptane, a 41 species, 266 elementary reactions chemical kinetic model is employed [18], which is consistent with that in [1]. For JP10, a 40 species 616 elementary reactions mechanism is used [19].

The post-shock conditions can be solved given a detonation velocity and the conditions of the initial state. These post-shock conditions are then used as the initial conditions for the system of ODEs shown above. The stiff and unsteady system of ODEs are numerically difficult to solve, but have been done successfully using the MATLAB ode113, MATLAB ode15s and scipy.integrate.solve_ivp LSODA integrators [20, 21]. The detonation velocity, however, is not known up front. It must be iterated until the downstream boundary condition is met.

The steady state solution can be obtained as follows. First, a guessed detonation velocity is used in conjunction with a numerical normal shock solver to determine the conditions of the post-shock state. These conditions are then used as initial conditions to solve the system of ODEs with respect to space until one of two conditions are satisfied: the integration reaches a certain pre-defined length, or the local Mach number reaches one. Depending on which condition marks the end of the domain, the detonation velocity is either increased or decreased. If the downstream gas state reaches a unity mach number, then the gas state is under-driven. This marks where the detonation Rayleigh and Hugoniot curves do not intersect on a Rankine-Hugoniot plot [2]. This leads to the local mach number reaching one, leading to a shock which propagates upstream, accelerating the already propagating shock. When the detonation velocity is too high, the gas state never reaches one, allowing downstream expansion waves to attenuate and slow the shock. The convergence of the two criterion marks the steady state solution and can be evaluated using a bracketing root finding method. Careful attention must be paid to prevent the mach number from exceeding one, as the denominator of Eq. 24 will become zero. Numerical integration past a mach number of unity leads to sudden divergence and unrealistic gas states.

IV. Results and Discussions

Observations on spray detonation structure are presented thorough parametric studies here. First, the one-dimensional detonation structure is shown at various droplet diameters and external loss coefficients. Then, the concept of detonation limit is shown, as well as its dependence on the droplet diameter. Lastly, we compare the two fuels and discuss the resulting differences and their causes.

A. 1D structure of spray detonation

A comparison in structure between liquid and prevaporized premixed fuel in the absence of losses can be seen in Fig. 2 for the JP10/air mixture. The gas fuel temperature profile shows a much quicker thermal runaway and a higher downstream temperature than that of the liquid fuel. The gas phase detonation requires no vaporization of fuel before combustion, so the ignition delay is significantly shorter. Also, the presence of liquid phase requires heat to facilitate vaporization. This results in the lower downstream temperature because of the additional energy requirement. This energy used for vaporization also results in less energy contributing to the forward propagation of the detonation, reducing the detonation velocity.

Interestingly, we see a lower post-shock temperature in the gaseous case, even with a higher detonation velocity. This happens because of the presence of fuel vapor in front of the shock. The fuel increases both the pre-shock c_v and c_p, but c_v increases faster resulting in a lower γ. The reduction in γ for prevaporized gas results in a lower sound-speed and therefore higher Mach number, suggesting that the postshock temperature should be higher. However, γ also has an influence on the progression of the gas state in the normal shock relations. This can be seen through analytical

solutions to normal shock temperature ratios shown by Anderson [22]. The effect of γ on normal shock temperature ratio outweighs the effect of the higher shock mach number, resulting in a lower post-shock temperature.

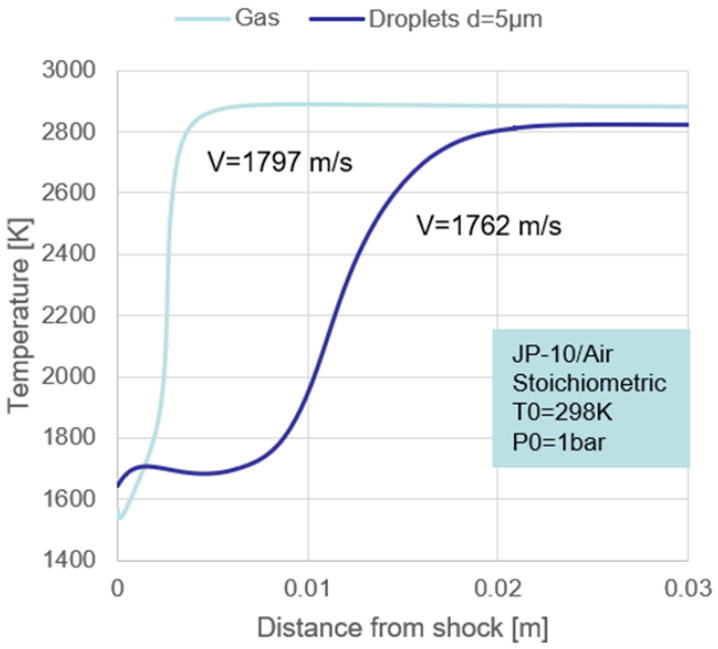

Fig. 2 A comparison of the detonation structure with liquid and pre-vaporized premixed fuel.

Figure 3 shows the effect of external losses on a spray detonation. A clear difference in post-shock temperature despite identical upstream gas conditions indicates differing detonation velocities. Both wall friction and wall heat loss result in velocity deficits. However, wall friction at $C_{d,w} = 0.03$ results in a greater velocity deficit than heat loss at a coefficient $C_{h,w} = 0.01$. Despite the greater velocity deficit, the downstream temperature of the friction loss case is actually higher than it is for the detonation with external heat loss.

The intersection of the two temperature profiles suggests non-linear effects of wall losses on the detonation structure. The presence of external heat loss, of course, results in a lower of downstream temperature. In the presence of friction losses, however, there is actually an introduction of kinetic energy to the flow through frictional work. Traditional stationary-frame arguments against frictional work do not hold in a moving reference frame, where the no-slip boundary applies to a moving wall [13]. This results in an influx of energy and momentum from the wall into the flow. The frictional contribution to the momentum equation, however, results in a net velocity deficit.

Detonation structures exhibit strong non-linearity as a function of droplet diameter, fuel type, and loss coefficients and therefore may have considerably different trends than those of $5\mu m$ diameter JP10 fuel shown in Fig. 3, as will be shown later.

B. Effects of droplet sizes on detonation limit

The detonation structures shown in subsection IV.A can be evaluated for a variety of external loss coefficients and a variety of droplet diameters for both fuels.

Fig. 4 displays the steady state velocity for heptane and JP10 under a variety of external drag conditions. First we note the existence of a steady state solution equal to the Chapman Jouguet speed when there is no friction present in the flow. As we increase the drag coefficients gradually, we notice the steady state velocity decreases. This makes intuitive sense and can also be explained analytically. Friction delays thermal runaway as shown in Fig. 3. This delay allows for an extended period over which the external losses can accumulate, resulting in a lower detonation velocity. Lee [2] discussed an identical curve for gaseous cases with external losses, as discussed in the introduction. The turning point of the curve represents the quenching point of the detonation. Solutions along the lower branch of the curve have been both experimentally and analytically proven to be unsteady in nature [2]. Figure 5 also shows an identical

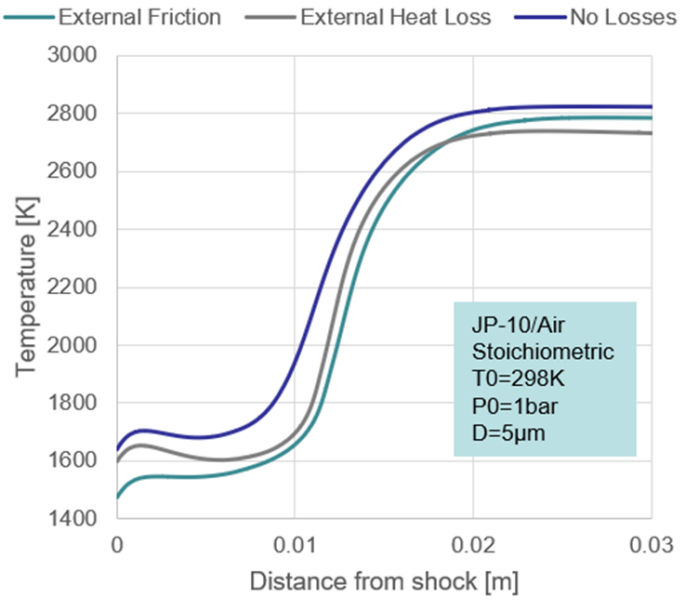

Fig. 3 Detonation structure under different external loss effects. The coefficient of friction ($C_{d,w}$) was chosen as 0.03, and the coefficient of heat loss ($C_{h,w}$) was chosen as 0.01.

comparison, but with varying heat loss. The heat loss induces an identical effect in both JP10 and heptane, with both seeing a reduction in detonation velocity as heat loss increases.

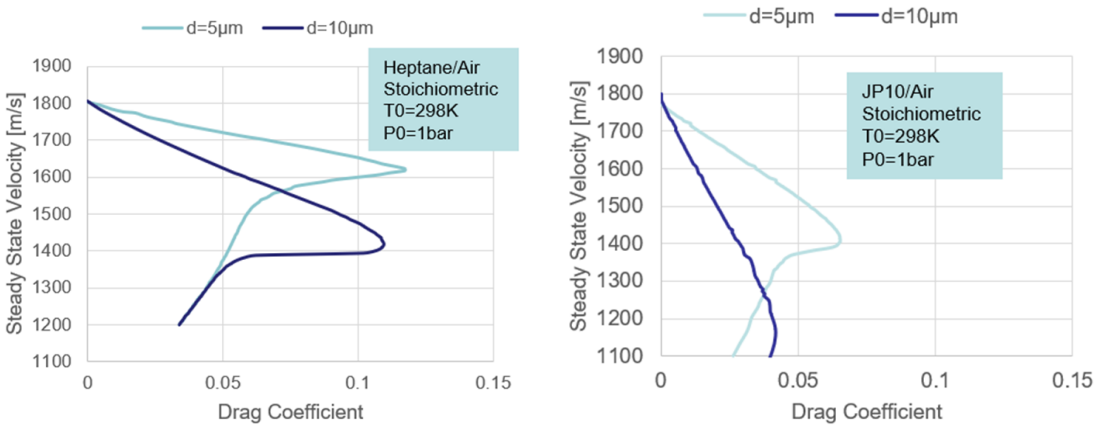

Fig. 4 Effect of external friction on heptane and JP10 detonation velocity for two droplet diameters.

C. Effects of fuel volatility

The presence of fuel in the liquid phase as well as external losses effects both heptane and JP10 in different ways. Figure 6 provides a comparison of heptane and JP-10 under equivalent drag coefficients and varying droplet diameters.

With heptane, we see the $5\mu m$ diameter droplet has the highest detonation velocity (very close to the Chapman-Jouguet velocity of $1804 m/s$), while the $1\mu m$ and $10\mu m$ diameter droplets have lower velocities. For the smallest droplet, we see a sharp drop in gas temperature immediately after the shock. The reason for this is the higher surface area to volume ratio of smaller droplets results in a greater acceleration from drag. The force of drag on the droplets varies as a function of surface area, according to Eq. 9, while the mass of the droplet varies as a function of volume, so the

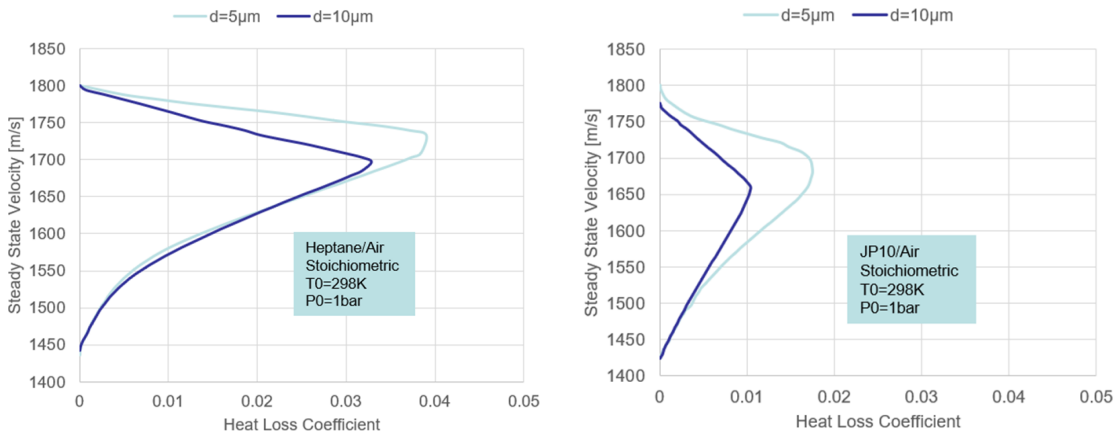

Fig. 5 Effect of external heat loss on heptane and JP10 detonation velocity for two droplet diameters.

F/m increases as diameter decreases, resulting in larger acceleration. This acceleration results in droplet congregation immediately behind the shock, which reduces the temperature of the gas as more energy is consumed to facilitate vaporization. This delays the onset of thermal runaway, which allows for a longer period of integrated loss due to friction. The net effect is a lower downstream temperature and a lower detonation velocity. In the $10\mu m$ diameter case, we again see a velocity deficit as well as a longer ignition delay. In this case, however, the delay results from the larger droplets limiting the rate of vaporization and ultimately limiting the rate of reaction.

The difference with JP10 is the $5\mu m$ is no longer reaches thermal runaway the fastest. The $1\mu m$ case, despite the droplet congregation again causing the first attempt at ignition to fail, still has a shorter ignition delay than the $5\mu m$ droplets. In this case, we see that the vaporization-limited reaction is already occurring in the $5\mu m$ droplets. The reason is related to the volatility of the fuels. This can be seen through the Antoine equations plotted in Fig. 7. The JP10 Antoine equation displays a significantly lower vapor pressure than heptane, indicating JP10 is relatively less volatile. JP10's lower vapor pressure induces vaporization-limited effects at smaller droplet diameters, resulting in changes to the optimal droplet size.

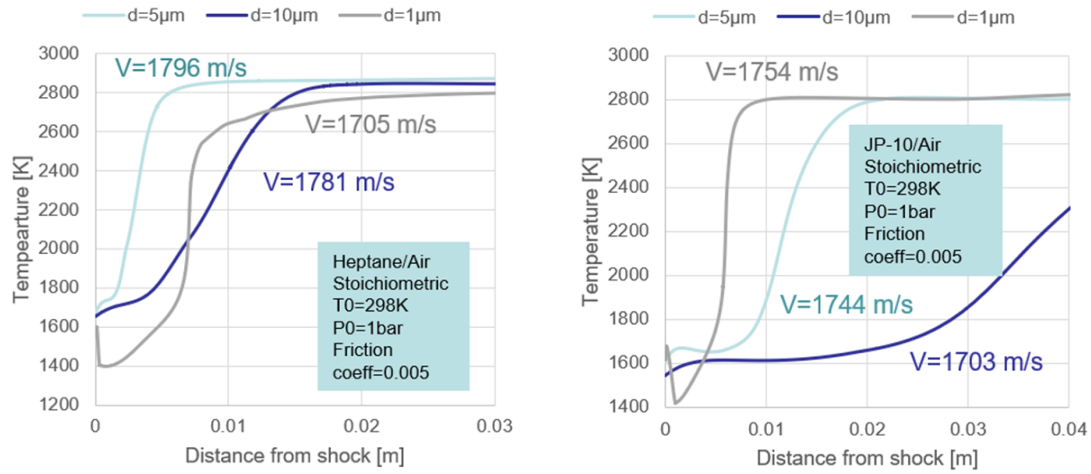

Fig. 6 One dimensional profiles of heptane and JP10 and their resulting detonation structures.

This phenomenon explains trends seen in Fig. 4. The lower vapor pressure fuel, JP10, displays greater velocity deficits at identical drag coefficients than heptane because the ignition delay is already higher due to the slower vaporization process. Any introduced wall drag will have a longer period of time to accumulate losses in the detonation structure.

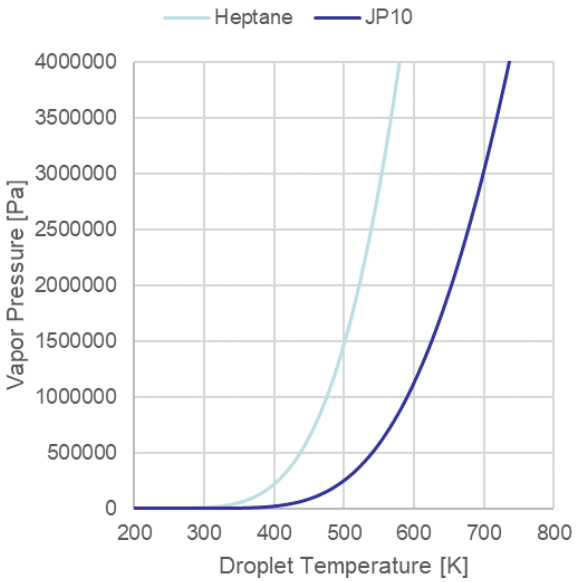

Fig. 7 Antoine equations for heptane and JP10.

V. Conclusions

A one dimensional model of ZND-type spray detonations was developed and solved using detailed chemistry and two-way coupling models. First the detonation structure was compared between gas and liquid phase detonation. It was noted that the reduction of detonation velocity and downstream temperature due to the enthalpy of vaporization of the fuel. Additionally, the effect of the presence of fuel in the pre-gas state resulted in a decreased post-shock temperature. Next, the effect of external heat and friction losses on the detonation was discussed. The introduction of friction losses causes an increase in ignition delay after the shock has passed, allowing for a longer period of integrated loss. External heat loss, similarly, results in a reduction in detonation velocity by reducing the chemical energy contributing to the forward propagation of the detonation. Both heat and friction losses reduce the temperature profile as a result of these velocity deficits. Higher loss coefficients are shown to inevitably lead to quenching as shown in Figs. 4 and 5, with the point of quenching defined as the point where the detonation can no longer propagate in a steady state.

Finally, a comparison between the two fuels was shown, highlighting the effect of volatility on the detonation structure and velocities. The volatile fuel, heptane, was shown to have its fastest heat release with $5\mu m$ diameter droplets, whereas the less volatile fuel, JP10, was shown to have its with the $1\mu m$ diameter fuel. JP10 also appeared to have vaporization-limited detonations at lower droplet diameters than heptane. As a result, heptane was shown to be more resilient to external losses due to its relatively short induction period resulting from its fast vaporization. Fast vaporization resulted in an earlier onset of thermal runaway, and less integrated losses from both heat and friction. JP10, however, was less resilient and was shown to have lower quenching points resulting from both friction and heat loss. The volatility of the fuel greatly affected the quenching resilience of the detonation to external losses.

References

[1] Lu, T., and Law, C. K., "Heterogeneous Effects in the Propagation and Quenching of Spray Detonations," *Journal of Propulsion and Power*, Vol. 20, 2004, pp. 820–827. https://doi.org/10.2514/1.5561.

[2] Lee, J. H. S., *The Detonation Phenomenon*, Cambridge University Press, 2008. https://doi.org/10.1017/CBO9780511754708.

[3] Eidelman, S., and Burcat, A., "Evolution of a detonation wave in a cloud of fuel droplets. I - Influence of igniting explosion," *AIAA Journal*, Vol. 18, 1980, pp. 1103–1109. https://doi.org/10.2514/3.7711.

[4] Gubin, S. A., and Sichel, M., "Calculation of the Detonation Velocity of a Mixture of Liquid Fuel Droplets and a Gaseous Oxidizer," *Combustion Science and Technology*, Vol. 17, 1977, pp. 109–117. https://doi.org/10.1080/00102207708946821.

[5] Pierce, T., and Nicholls, J., "Time variation in the reaction-zone structure of two-phase spray detonations," *Symposium (International) on Combustion*, Vol. 14, 1973, pp. 1277–1284. https://doi.org/10.1016/S0082-0784(73)80114-6.

[6] Borisov, A. A., Gel'fand, B. E., Gubin, S. A., Kogarko, S. M., and Podgrebenkov, A. L., "Detonation reaction zone in two-phase mixtures," *Combustion, Explosion, and Shock Waves*, Vol. 6, 1970, pp. 327–336. https://doi.org/10.1007/BF00742508.

[7] Kailasanath, K., "Liquid-Fueled Detonations in Tubes," *Journal of Propulsion and Power*, Vol. 22, 2006, pp. 1261–1268. https://doi.org/10.2514/1.19624.

[8] Nguyen, V. B., Teo, C. J., Chang, P.-H., Li, J. M., and Khoo, B. C., "Numerical investigation of the liquid-fueled pulse detonation engine for different operating conditions," *Shock Waves*, Vol. 29, 2019, pp. 1205–1225. https://doi.org/10.1007/s00193-019-00898-z.

[9] Taylor, B., Kessler, D., Gamezo, V., and Oran, E., "Numerical simulations of hydrogen detonations with detailed chemical kinetics," *Proceedings of the Combustion Institute*, Vol. 34, 2013, pp. 2009–2016. https://doi.org/10.1016/j.proci.2012.05.045.

[10] Cheatham, S., and Kailasanath, K., "Numerical modelling of liquid-fuelled detonations in tubes," *Combustion Theory and Modelling*, Vol. 9, 2005, pp. 23–48. https://doi.org/10.1080/13647830500051786.

[11] Cheatham, S., and Kailasanath, K., "Single-Cycle Performance of Idealized Liquid-Fueled Pulse Detonation Engines," *AIAA Journal*, Vol. 43, 2005, pp. 1276–1283. https://doi.org/10.2514/1.11799.

[12] Zel'dovich, Y. B., Gel'fand, B. E., Kazhdan, Y. M., and Frolov, S. M., "Detonation propagation in a rough tube taking account of deceleration and heat transfer," *Combustion, Explosion, and Shock Waves*, Vol. 23, 1987, pp. 342–349. https://doi.org/10.1007/BF00748797.

[13] Higgins, A., "Steady One-Dimensional Detonations," , 2012. https://doi.org/10.1007/978-3-642-22967-1_2.

[14] Guo, Y., Yang, F., Xing, Y., Li, D., Fang, W., and Lin, R., "Bubble-Point Vapor Pressure Measurement for System JP-10 and Tributylamine by an Inclined Ebulliometer," *Energy Fuels*, Vol. 22, 2008, pp. 510–513. https://doi.org/10.1021/ef700396k.

[15] Chickos, J. S., Hillesheim, D., Nichols, G., and Zehe, M. J., "The enthalpies of vaporization and sublimation of exo- and endo-tetrahydrodicyclopentadienes at T=298.15K," *The Journal of Chemical Thermodynamics*, Vol. 34, 2002, pp. 1647–1658. https://doi.org/10.1016/S0021-9614(02)00229-X.

[16] Bruno, T., Huber, M., Laesecke, A., Lemmon, E., and Perkins, R., "Thermochemical and Thermophysical Properties of JP-10," , 6 2006.

[17] Goodwin, D. G., Speth, R. L., Moffat, H. K., and Weber, B. W., "Cantera: An Object-oriented Software Toolkit for Chemical Kinetics, Thermodynamics, and Transport Processes," https://www.cantera.org, 2021. https://doi.org/10.5281/zenodo.4527812, version 2.5.1.

[18] Held, T. J., Marchese, A. J., and Dryer, F. L., "A Semi-Empirical Reaction Mechanism for n-Heptane Oxidation and Pyrolysis," *Combustion Science and Technology*, Vol. 123, 1997, pp. 107–146. https://doi.org/10.1080/00102209708935624.

[19] Tao, Y., Xu, R., Wang, K., Shao, J., Johnson, S. E., Movaghar, A., Han, X., Park, J.-W., Lu, T., Brezinsky, K., Egolfopoulos, F. N., Davidson, D. F., Hanson, R. K., Bowman, C. T., and Wang, H., "A Physics-based approach to modeling real-fuel combustion chemistry – III. Reaction kinetic model of JP10," *Combustion and Flame*, Vol. 198, 2018, pp. 466–476. https://doi.org/10.1016/j.combustflame.2018.08.022.

[20] Petzold, L., "Automatic Selection of Methods for Solving Stiff and Nonstiff Systems of Ordinary Differential Equations," *SIAM Journal on Scientific and Statistical Computing*, Vol. 4, 1983. https://doi.org/10.1137/0904010.

[21] Shampine, L. F., and Reichelt, M. W., "The MATLAB ODE Suite," *SIAM Journal on Scientific Computing*, Vol. 18, 1997, pp. 1–22. https://doi.org/10.1137/S1064827594276424.

[22] Anderson, J., *Modern Compressible Flow*, 3rd ed., McGraw-Hill, 2003.